Mass-transport limitations in spot-based microarrays

Ming Zhao,[1,2] Xuefeng Wang,[1,3] and David Nolte[1,*]

[1]*Department of Physics, Purdue University, 525 Northwestern Avenue, West Lafayette, IN 47907, USA*
[2]*Currently with the College of Optical Sciences, the University of Arizona, 1630 East University Boulevard, Tucson, AZ 85721, USA*
[3]*Currently with the Department of Physics, University of Illinois at Urbana-Champaign, 1110 West Green Street, Urbana, IL 61801, USA*
**nolte@purdue.edu*

Abstract: Mass transport of analyte to surface-immobilized affinity reagents is the fundamental bottleneck for sensitive detection in solid-support microarrays and biosensors. Analyte depletion in the volume adjacent to the sensor causes deviation from ideal association, significantly slows down reaction kinetics, and causes inhomogeneous binding across the sensor surface. In this paper we use high-resolution molecular interferometric imaging (MI2), a label-free optical interferometry technique for direct detection of molecular films, to study the inhomogeneous distribution of intra-spot binding across 100 micron-diameter protein spots. By measuring intra-spot binding inhomogeneity, reaction kinetics can be determined accurately when combined with a numerical three-dimensional finite element model. To ensure homogeneous binding across a spot, a critical flow rate is identified in terms of the association rate k_a and the spot diameter. The binding inhomogeneity across a spot can be used to distinguish high-affinity low-concentration specific reactions from low-affinity high-concentration non-specific binding of background proteins.

OCIS codes: (180.3170) Interference microscopy; (280.1415) Biological sensing and sensors; (280.4788) Optical sensing and sensors; (240.6645) Surface differential reflectance; (170.1470) Blood or tissue constituent monitoring; (170.0110) Imaging systems.

References and links

1. S. F. Kingsmore, "Multiplexed protein measurement: technologies and applications of protein and antibody arrays," Nat. Rev. Drug Discov. **5**(4), 310–321 (2006).
2. G. MacBeath, "Protein microarrays and proteomics," Nat. Genet. **32**(Suppl), 526–532 (2002).
3. L. L. Lv, and B. C. Liu, "High-throughput antibody microarrays for quantitative proteomic analysis," Expert Rev. Proteomics **4**(4), 505–513 (2007).
4. H. Zhu, and M. Snyder, "Protein chip technology," Curr. Opin. Chem. Biol. **7**(1), 55–63 (2003).
5. M. A. Cooper, "Optical biosensors in drug discovery," Nat. Rev. Drug Discov. **1**(7), 515–528 (2002).
6. N. Ramachandran, S. Srivastava, and J. LaBaer, "Applications of protein microarrays for biomarker discovery," Proteom. Clin. Appl. **2**(10–11), 1444–1459 (2008).
7. A. Brecht, and G. Gauglitz, "Optical probes and transducers," Biosens. Bioelectron. **10**(9-10), 923–936 (1995).
8. G. Gauglitz, "Direct optical sensors: principles and selected applications," Anal. Bioanal. Chem. **381**(1), 141–155 (2005).
9. X. D. Fan, I. M. White, S. I. Shopova, H. Y. Zhu, J. D. Suter, and Y. Z. Sun, "Sensitive optical biosensors for unlabeled targets: a review," Anal. Chim. Acta **620**(1-2), 8–26 (2008).
10. D. D. Nolte, "Invited Review Article: Review of centrifugal microfluidic and bio-optical disks," Rev. Sci. Instrum. **80**(10), 101101 (2009).
11. E. Özkumur, A. Yalçin, M. Cretich, C. A. Lopez, D. A. Bergstein, B. B. Goldberg, M. Chiari, and M. S. Unlü, "Quantification of DNA and protein adsorption by optical phase shift," Biosens. Bioelectron. **25**(1), 167–172 (2009).
12. J. N. Anker, W. P. Hall, O. Lyandres, N. C. Shah, J. Zhao, and R. P. Van Duyne, "Biosensing with plasmonic nanosensors," Nat. Mater. **7**(6), 442–453 (2008).

#132716 - $15.00 USD Received 2 Aug 2010; revised 16 Sep 2010; accepted 17 Sep 2010; published 20 Sep 2010

13. A. Yalcin, K. C. Popat, J. C. Aldridge, T. A. Desai, J. Hryniewicz, N. Chbouki, B. E. Little, Oliver King, V. Van, Sai Chu, D. Gill, M. Anthes-Washburn, M. S. Unlu, and B. B. Goldberg, "Optical sensing of biomolecules using microring resonators," IEEE J. Sel. Top. Quantum Electron. **12**(1), 148–155 (2006).
14. G. Shekhawat, S. H. Tark, and V. P. Dravid, "MOSFET-Embedded microcantilevers for measuring deflection in biomolecular sensors," Science **311**(5767), 1592–1595 (2006).
15. L. Rindorf, J. B. Jensen, M. Dufva, L. H. Pedersen, P. E. Høiby, and O. Bang, "Photonic crystal fiber long-period gratings for biochemical sensing," Opt. Express **14**(18), 8224–8231 (2006).
16. S. L. Seurynck-Servoss, A. M. White, C. L. Baird, K. D. Rodland, and R. C. Zangar, "Evaluation of surface chemistries for antibody microarrays," Anal. Biochem. **371**(1), 105–115 (2007).
17. W. Kusnezow, and J. D. Hoheisel, "Solid supports for microarray immunoassays," J. Mol. Recognit. **16**(4), 165–176 (2003).
18. U. B. Nielsen, and B. H. Geierstanger, "Multiplexed sandwich assays in microarray format," J. Immunol. Methods **290**(1-2), 107–120 (2004).
19. B. B. Haab, "Antibody arrays in cancer research," Mol. Cell. Proteomics **4**(4), 377–383 (2005).
20. P. Angenendt, "Progress in protein and antibody microarray technology," Drug Discov. Today **10**(7), 503–511 (2005).
21. P. R. Nair, and M. A. Alam, "Theory of "Selectivity" of label-free nanobiosensors: A geometro-physical perspective," J. Appl. Phys. **107**(6), 064701 (2010).
22. R. P. Ekins, "Ligand assays: from electrophoresis to miniaturized microarrays," Clin. Chem. **44**(9), 2015–2030 (1998).
23. P. R. Nair, and M. A. Alam, "Performance limits of nanobiosensors," Appl. Phys. Lett. **88**(23), 233120 (2006).
24. W. Kusnezow, Y. V. Syagailo, S. Rüffer, N. Baudenstiel, C. Gauer, J. D. Hoheisel, D. Wild, and I. Goychuk, "Optimal design of microarray immunoassays to compensate for kinetic limitations: theory and experiment," Mol. Cell. Proteomics **5**(9), 1681–1696 (2006).
25. P. Schuck, and A. P. Minton, "Analysis of mass transport-limited binding kinetics in evanescent wave biosensors," Anal. Biochem. **240**(2), 262–272 (1996).
26. P. Schuck, "Kinetics of ligand binding to receptor immobilized in a polymer matrix, as detected with an evanescent wave biosensor. I. A computer simulation of the influence of mass transport," Biophys. J. **70**(3), 1230–1249 (1996).
27. P. E. Sheehan, and L. J. Whitman, "Detection limits for nanoscale biosensors," Nano Lett. **5**(4), 803–807 (2005).
28. W. Kusnezow, Y. V. Syagailo, I. Goychuk, J. D. Hoheisel, and D. G. Wild, "Antibody microarrays: the crucial impact of mass transport on assay kinetics and sensitivity," Expert Rev. Mol. Diagn. **6**(1), 111–124 (2006).
29. W. Kusnezow, Y. V. Syagailo, S. Rüffer, K. Klenin, W. Sebald, J. D. Hoheisel, C. Gauer, and I. Goychuk, "Kinetics of antigen binding to antibody microspots: strong limitation by mass transport to the surface," Proteomics **6**(3), 794–803 (2006).
30. G. Q. Hu, Y. L. Gao, and D. Q. Li, "Modeling micropatterned antigen-antibody binding kinetics in a microfluidic chip," Biosens. Bioelectron. **22**(7), 1403–1409 (2007).
31. X. F. Wang, M. Zhao, and D. D. Nolte, "Area-scaling of interferometric and fluorescent detection of protein on antibody microarrays," Biosens. Bioelectron. **24**(4), 981–993 (2008).
32. M. Zhao, X. F. Wang, G. M. Lawrence, P. Espinoza, and D. D. Nolte, "Molecular interferometric imaging for biosensor applications," IEEE J. Sel. Top. Quantum Electron. **13**(6), 1680–1690 (2007).
33. M. Zhao, X. F. Wang, and D. D. Nolte, "Molecular interferometric imaging," Opt. Express **16**(10), 7102–7118 (2008).
34. X. F. Wang, M. Zhao, and D. D. Nolte, "Common-path interferometric detection of protein monolayer on the BioCD," Appl. Opt. **46**(32), 7836–7849 (2007).
35. M. Zhao, D. D. Nolte, W. R. Cho, F. Regnier, M. Varma, G. Lawrence, and J. Pasqua, "High-speed interferometric detection of label-free immunoassays on the biological compact disc," Clin. Chem. **52**(11), 2135–2140 (2006).
36. M. Eliasson, A. Olsson, E. Palmcrantz, K. Wiberg, M. Inganäs, B. Guss, M. Lindberg, and M. Uhlén, "Chimeric IgG-binding receptors engineered from staphylococcal protein A and streptococcal protein G," J. Biol. Chem. **263**(9), 4323–4327 (1988).
37. K. P. S. Dancil, D. P. Greiner, and M. J. Sailor, "A porous silicon optical biosensor: Detection of reversible binding of IgG to a protein A-modified surface," J. Am. Chem. Soc. **121**(34), 7925–7930 (1999).
38. O. C. Zienkiewicz, and R. L. Taylor, *The Finite Element Method, 5th edition* (Butterworth-Heinemann, 2000).
39. T. Jøssang, J. Feder, and E. Rosenqvist, "Photon correlation spectroscopy of human IgG," J. Protein Chem. **7**(2), 165–171 (1988).

1. Introduction

Microarrays are high-throughput analytical platforms for the detection of target molecules in a biological sample. In a solid-support microarray, multiple affinity reagents are printed as spots onto a solid substrate. When incubated against a biological sample, the surface-immobilized affinity reagents react with their specific target analytes. With the capability of high-throughput detection of multiple analytes at low cost and high sensitivity, microarray technology has great potential in system-oriented proteomics [1–4], drug discovery [5] and multiplexed medical diagnostics [6]. Progress on new detection schemes [7–15], surface

#132716 - $15.00 USD Received 2 Aug 2010; revised 16 Sep 2010; accepted 17 Sep 2010; published 20 Sep 2010

chemistries and immobilization strategies [16,17] and assay formats [18–20] are improving microarray reliability. However, the capability of current protein microarray technology for large-scale profiling of complicated biological samples is still limited, and many technical challenges remain that significantly limit the detection sensitivity of microarray immunoassays [21].

The theoretical detection sensitivity of antibody microarrays can be predicted by the ambient-analyte theory [22], which shows that the equilibrium binding site occupancy in a microarray immunoassay would depend only on the analyte concentration, provided that the amount of antibody is small and the binding of analyte to the antibody spots does not significantly affect the bulk concentration. Under these conditions, with picomolar affinity antibodies and a detection system with a signal-to-noise ratio of 1000:1, femtomolar level detection sensitivity could be reached, but few systems have ever reached such sensitivity [23], and they often rely on signal amplification.

This discrepancy between the theoretical and experimental assay sensitivity is caused by mass transport limitation. The ambient-analyte theory makes the assumption that the analyte concentration is not significantly affected by the capture process. However, in practical assays antibodies are often immobilized in microspots at a high surface density, which leads to high capture rate of analyte. When the analyte capture rate is faster than the analyte replenishment rate through mass transport, the analyte concentration is depleted locally adjacent to the antibody spots, and the reaction deviates from the ambient-analyte condition. The depletion of analyte drives the reaction away from ideal association, slows down the reaction and reduces the amount of captured analyte, possibly by orders of magnitude, and causes inhomogeneous analyte binding as analyte concentration varies across the antibody microspots. Among the technical challenges surface-based protein microarray technology faces, the mass-transport limitation of target analyte from sample solution to the sensor surface may be the *primary* limitation of current solid-support microarray immunoassays [24]. Because of this, mass-transport-limited reaction kinetics have been studied extensively, by theoretical [25–27], experimental [24,28,29] and computational [30] approaches. However, all these previous studies have focused on the *average* response over the sensor surface [31] and have not addressed the analyte binding inhomogeneity within the sensor surface, which is closely related to the analyte concentration gradient and is the origin of the deviations from ideal association.

In this paper, we employ the diffraction-limited spatial resolution of molecular interferometric imaging [32] to study mass-transport-induced analyte binding inhomogeneity within single 100 micron diameter protein spots. Binding under commonly encountered conditions leads to pronounced binding inhomogeneity within the spots. A three-dimensional finite element computational model is compared with the experimental results and is used to explore regions of the reaction kinetics parameter space that are not easily accessible to experiments. We show that, in the low concentration limit, the shapes of the mass-transport-induced reaction inhomogeneities are independent of analyte concentration, and we present guidelines to optimize a microarray immunoassay through the choice of the size of an antibody microspot and the sample flow rate. Finally, we propose a possible use of mass-transport-induced reaction inhomogeneity to distinguish high-affinity low-concentration specific reactions from low-affinity high-concentration non-specific binding of background proteins.

2. Molecular interferometric imaging

2.1 Molecular films

Molecular interferometric imaging is a sensitive detection platform for label-free interferometric detection of surface-immobilized biomolecules [32,33]. MI2 is based on normal-incidence inline common-path quadrature interferometry [34] combined with far-field optical imaging. An oxide layer on silicon acts as a spacer layer, and interference between partial reflections from the bottom of the spacer layer and immobilized biomolecules on top

#132716 - $15.00 USD Received 2 Aug 2010; revised 16 Sep 2010; accepted 17 Sep 2010; published 20 Sep 2010

produces intensity modulation that can be detected directly in the far field by a pixel-array detector on the image plane of the optical system. The signal and reference waves are produced locally and share the same optical path, making the interferometry ultra-stable.

The interference between the reflected partial waves changes the reflection coefficient of the substrate when protein is present. By designing the amplitude and phase of the substrate reflection coefficient, the protein-induced reflectance change can be maximized. One simple substrate is an oxide-on-silicon two-layer substrate, with a thickness at or near the condition of phase-quadrature that imprints a relative phase of $\pi/2$ between the partial reflections from the top and bottom interface of the oxide layer [35]. The relative reflectance change caused by the presence of protein is given by

$$\frac{\Delta I}{I} = C(\lambda, d)\left(g^2(x, y) \otimes h(x, y)\right) \tag{1}$$

where g^2 is the normalized point-spread function of the imaging system and $h(x,y)$ is the protein height function on the substrate surface. The coefficient $C(\lambda,d)$ that gives the conversion from biolayer height to intensity is [34]

$$C(\lambda, d) = \frac{8\pi n_p}{\lambda} \mathrm{Im}\left(\frac{(r_p - r)(1 - r r_p)}{1 - r_p^2}\right) \tag{2}$$

where n_p is the refractive index of protein, r is the reflection coefficient of the substrate (immersed in medium) and r_p is the reflection coefficient of the medium-protein interface. A measured change in the relative intensity can be converted to surface protein height using this conversion coefficient. A background normalization procedure is used to remove the spatial variation in the illumination background to obtain the relative intensity changes caused by protein. Two images of the same sample are taken either with a time shift or spatial shift, and then are referenced against each other by calculating the normalized difference between the image pairs [32]. This procedure completely removes the spatial inhomogeneity in the illumination, and the resulting measurement of protein-induced relative intensity change is limited only by the shot-noise of the CCD detector.

2.2. Experimental procedures

In MI2, we measure the reflectance change caused by the surface immobilized protein molecules directly with an imaging system [33]. We use 100 mm diameter silicon wafers with a top oxide layer as support, and choose the thickness of the oxide layer to be 120 nm. At this oxide thickness, the protein-induced relative reflectance change is optimized for 630 nm wavelength incident light. The reflectance change caused by protein molecules under these conditions is positive, making it easy to distinguish from scattering loss by particle debris.

The oxide surface is activated with an aldehyde surface chemistry that covalently binds protein molecules. The wafer surface is partitioned into 96 independent wells using hydrophobic ink. Protein spots are then printed into these wells by a Piezo ink-jet protein printer (Scienion Inc., distributed by BioDot) onto the substrate in 300 pL drops, resulting in about 100 micron diameter printed protein spots. The printing procedure was optimized to produce uniform protein spots. A 2x2 unit cell pattern of protein spots is used for the experiments, in which two target and two reference protein spots are printed on opposite diagonals to form a single unit cell. This format provides good rejection of systematic drifts and common non-specific binding to both groups of spots. For each well, 16 unit cells are printed, resulting in an 8x8 protein spot array.

The optical setup of the MI2 detection system consists of a monochromic light source, a reflective microscope and a CCD camera. The light source we used is a 10 mW red LED (eLED.com) with center wavelength at 630 nm and a bandwidth of 30 nm. The LED is very stable with low intensity drift over time. Light is directed from the light source into a reflective microscope (Leica DMR) and focused onto the sample by objectives with 7x, 20x or

#132716 - $15.00 USD Received 2 Aug 2010; revised 16 Sep 2010; accepted 17 Sep 2010; published 20 Sep 2010

40x magnification. Reflected light from the sample is collected by the same objective and imaged onto a CCD camera (QImaging 4000R) and captured to a computer.

A flow cell is constructed by attaching an anti-reflection coated (center wave-length 630 nm, reflectance < 0.1% at 630 nm) 18x18x0.17 mm cover slide by double-sided tape on top of one well on a disc. The resulting height of the flow cell is approximately 0.2 mm. Sample solution is driven into the flow cell from one side of the cover slide and drained from the opposite side, with the flow rate controlled by a syringe pump (New Era NE500). The printed protein spots and the surface of the disc are imaged through the cover slide and the sample solution by the microscope system. The images taken at different times are referenced to the first image by calculating the normalized difference of the two images, using

$$D_{ij}(t) = 2\frac{I_{ij}(t) - I_{ij}(0)}{I_{ij}(t) + I_{ij}(0)} = C(\lambda, d)\left(h_{ij}(t) - h_{ij}(0)\right) \tag{3}$$

in which the subscript *i*,*j* denotes the pixel number in the imaging system. The normalized difference removes spatial inhomogeneity in the illumination background, and the result is proportional to the protein height change during the incubation. The measurement of the protein height change is then limited by the photon shot-noise from the CCD camera [27].

3. Experimental results

3.1 Flow rate dependence

To study the effect of the flow velocity on mass-transport-limited reactions, the binding of the Fc region of rabbit IgG against protein A/G was studied under different flow rates. Protein A/G is a fusion protein that contains the IgG-binding domain from protein A and protein G, and specifically binds only the Fc region of IgG molecules [36,37]. Protein A/G was printed in the 2x2 unit cell pattern described in the previous section, with chicken IgY spots serving as reference. 32 protein A/G spots and 32 reference spots were printed in a single array, which was then incubated and measured in a flow cell. The sample solution we used for this experiment was 200 ng/mL rabbit IgG prepared in pH 7.4 phosphate buffered saline (PBS), with 2 μg/mL bovine serum albumin as a non-specific protein background. The sample was introduced into the flow cell with continuous flow at velocities ranging from 5 μm/sec to 50 μm/sec. After each incubation, rabbit IgG was eluted from the protein A/G with a pH 3.0 100 mM glycine-HCl buffer solution.

Binding of rabbit IgG to protein A/G through the Fc region was imaged at a rate of one measurement every 40 seconds. For each measurement frame, the responses from the 32 protein A/G spots were spatially averaged together to reduce the detection shot noise of the CCD. The results are shown in Fig. 1 (Media 1) as a combined movie of the average binding inhomogeneity profile of rabbit IgG within the 120 micron diameter protein A/G spots when they were incubated under four different flow conditions. The flow rates in the movie are: top-left 5 μm/sec; top-right 10 μm/sec; bottom-left 20 μm/sec; bottom-right 50 μm/sec. The data in the movie were acquired and averaged over the same set of protein spots in the same flow cell from four consecutive experiments with different flow rates. After each incubation, the rabbit IgG was eluted and the printed protein A/G spots were reused for the next incubation. No significant loss of protein activity was observed in this process.

From Fig. 1, binding of analyte at the leading edge of the protein spots was pronounced at low velocity, caused by the depletion of analyte as the sample travelled across the protein spot. Diffusion-enhanced binding also occurs at the sides and the trailing edge of the spots, which also is more apparent at low flow velocities. The width of the leading binding edge increases with increasing flow velocity, producing more uniform binding across the spot under flow rates above 20 μm/sec.

#132716 - $15.00 USD Received 2 Aug 2010; revised 16 Sep 2010; accepted 17 Sep 2010; published 20 Sep 2010

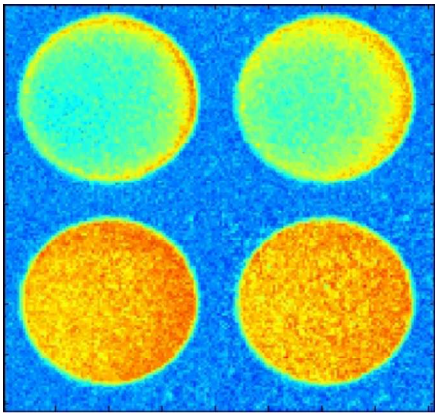

Fig. 1. (Media 1) Movie of 200 ng/mL rabbit IgG binding against protein A/G under different flow rates of: top-left 5 μm/sec; top-right 10 μm/sec; bottom-left 20 μm/sec; bottom-right 50 μm/sec. Pronounced edge binding due to mass transport is observed at low flow velocities. The flow direction is from the upper right to lower left.

When the analyte binding is averaged over the entire protein spot at low flow rates, the deficient binding in the center of the spots leads to a large deviation from the ideal association process. The spot-averaged binding is shown in Fig. 2(a). At flow rates below 20 μm/sec analyte depletion from the sample suppresses binding in the center of the spot. However, when only the binding at the leading edges of the protein spots are used, the protein bindings under different flow rates are almost identical, as shown in Fig. 2(b). This is because the leading edges are always exposed to the bulk concentration of analyte.

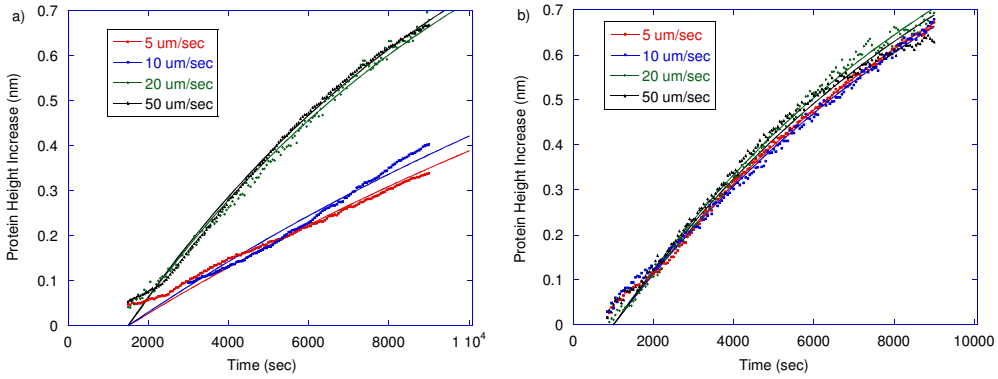

Fig. 2. Height increase of the protein spots at different flow rates (a) averaged over the full spot, large deviations occur at low flow rates; (b) from only the leading edges of the protein spots.

When the spot-averaged response is fitted to the ideal association equation, the resulting k_a can vary by more than 50%, as shown in Fig. 3. The leading edge produces much smaller variation, in which the resulting k_a values deviate by less than 5%. Therefore, by analyzing the leading edge of the protein spots (or by reducing the size of the spots [15,17]), the reaction kinetics can be measured more precisely.

#132716 - $15.00 USD Received 2 Aug 2010; revised 16 Sep 2010; accepted 17 Sep 2010; published 20 Sep 2010

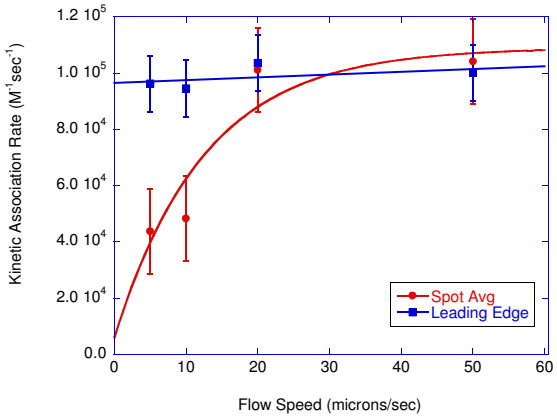

Fig. 3. Association rate k_a from fits to ideal association for the full-spot average compared with signals taken only from the leading edge of the spots.

3.2 Kinetic association rate dependence

The pronounced leading edge caused by analyte depletion depends on the kinetic association rates as well as the flow rate. To study the effect of the kinetic association rate on the mass-transport-limited reaction, three different molecular binding systems were studied that had different k_a. These were: (a) the association of streptavidin (53 kDa) to biotin (k_a = 1x10^6 M^{-1}sec^{-1}); (b) the association of rabbit IgG (150 kDa) to protein A/G bound through the Fc region (k_a = 1x10^5 M^{-1}sec^{-1}); and (c) non-specific association of bovine serum albumin (BSA, 66 kDa)) to protein A/G (k_a = 1x10^2 M^{-1}sec^{-1}). The concentration of rabbit IgG and streptavidin for the specific binding experiments was 1 μg/mL, while the concentration of BSA for the non-specific binding was much higher at 200 μg/mL. A 50 μm/sec flow rate was used for all three reactions. The resulting spot binding inhomogeneity is shown in Fig. 4. The data shown were selected when the spots showed the largest intraspot variations. A higher association rate leads to a larger concentration gradient and binding inhomogeneity across a protein spot. Therefore, by measuring the inhomogeneity of the protein spot profile, it is possible to separate specific association at high affinity from non-specific association at lower affinity. High-affinity specific associations produce steep leading edges in the direction of the flow and large inhomogeneity across the spot, while low-affinity non-specific binding across the spot is uniform. When different flow velocities are used, high-affinity associations show a strong dependence on flow velocity in the binding profile, while low-affinity associations do not depend significantly on flow velocities because the reactions at low affinity are not mass-transport limited.

#132716 - $15.00 USD Received 2 Aug 2010; revised 16 Sep 2010; accepted 17 Sep 2010; published 20 Sep 2010

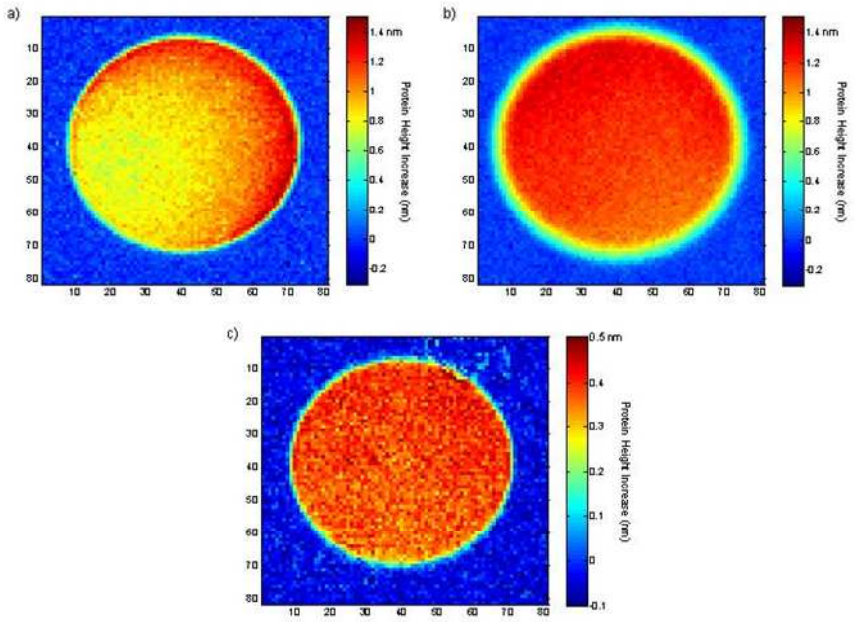

Fig. 4. Binding inhomogeneity in (a) 1 μg/mL streptavidin binding to immobilized biotinylated anti-rabbit IgG, (b) 1 μg/mL rabbit IgG binding to immobilized protein A/G, and (c) 200 μg/mL BSA binding non-specifically to protein A/G. The flow velocity for all experiments was 50 μm/sec. The mass-transport effect is more obvious in larger k_a reactions because of faster analyte depletion.

4. Numerical modeling

4.1 Numerical model of mass transport limited reaction

Molecular interferometric imaging measures the optical phase shift from surface immobilized biomolecules, which is converted to a surface height profile. For a binding reaction between an immobilized capture reagent and its target analyte in sample solution, the surface height increase is given by

$$\frac{dH}{dt} = k_a C(H_{\max} - H) - k_d H \tag{4}$$

where $H_{\max}$ is the saturation protein height increase, which is proportional to surface binding site density, and C is the mass concentration of the analyte near the sensor surface. The association and dissociation rate constants of the reaction are k_a and k_d, respectively. If the analyte concentration stays constant in time, then the above equation is solved for ideal association,

$$H(t) = \frac{k_a C}{k_a C + k_d} H_{\max}\left[1 - \exp\left(-(k_d + k_a C)t\right)\right] \tag{5}$$

However, in a practical assay, the binding of analytes to the surface-immobilized capture reagents changes the analyte concentration, which changes the reaction from ideal association. The mass transport of analyte then comes into effect when the concentration becomes non uniform, and can be described by

$$\frac{\partial C}{\partial t} = -\vec{v} \cdot \nabla C + D\nabla^2 C \tag{6}$$

#132716 - $15.00 USD Received 2 Aug 2010; revised 16 Sep 2010; accepted 17 Sep 2010; published 20 Sep 2010

where v is the flow velocity, and D is the diffusion coefficient of the protein molecules. The boundary condition at the reaction surface as a result of mass conservation of the analyte is given in terms of the mass flux

$$D\frac{\partial C}{\partial z} = -\frac{\rho dH}{dt} \tag{7}$$

where ρ is the mass density of the analyte layer.

For the numerical study, the boundary condition can be introduced into the differential equation at the boundary through

$$\frac{\Delta C}{\Delta t} = -\vec{v}\cdot\nabla C + D\nabla^2 C - R\frac{\Delta H}{\Delta t} \tag{8}$$

where R is a conversion ratio between surface height increase and analyte concentration change, given by

$$R = \frac{\Delta C}{\Delta H} = \frac{\rho}{\Delta l} = \frac{\rho}{\sqrt{D}} \tag{9}$$

in which Δl is the height of the sample volume in which the analyte molecules can reach the sensor surface in unit time. Equation (8) contains both a mass transport term and a binding term and is numerically equivalent to Eq. (6) and Eq. (7).

From Eq. (8), it is clear that if there is analyte binding, then C cannot remain uniform across the sensor surface, because if C is a constant, then $\Delta C/\Delta t = -R\Delta H/\Delta t$, and the analyte concentration has a finite time derivative. If an assay begins from a uniform bulk concentration, then a concentration gradient will be established across the sensor surface until the mass transport rate of the analyte equals to the binding rate. Because analyte association is directly proportional to concentration, this concentration gradient will cause inhomogeneous association of the analyte across the sensor surface, which leads to deviations from the ideal association of Eq. (5).

We applied a three-dimensional finite element method [38] to solve the partial differential equation and to simulate the reactions described by Eq. (8) over a protein spot. In the FEM model, the binding of analyte and mass transport were calculated separately. For each time step, the analyte binding height dH was calculated by a finite difference method to solve Eq. (4), and analyte was removed from the adjacent sample volume. The finite element simulation then solved for the analyte concentration C from Eq. (6) in bulk solution. A parabolic velocity profile was used for pressure-driven flow across the flow cell,

$$v(z) = 6v_m(z/h)(1-z/h) \tag{10}$$

where v_m is the average flow velocity and h is the height of the flow cell. Additional boundary conditions used for the simulations are, $C = C_b$ at $t = 0$, $C = C_b$ at the inlet port of the fluidic channel, and $\vec{n}\cdot(D\vec{\nabla}C) = 0$ at all other boundaries.

4.2 Validation of FEM simulations

The FEM simulation was compared with experimental results for validation. Figure 5 shows the comparison of the simulation with experimental results. A movie of the comparison between experimental data and simulation is shown in Fig. 5(a) (Media 2) for the association of rabbit IgG against protein A/G after 2 hours of incubation. The parameters for the reaction were a kinetic association rate k_a = 1x10^5 M^{-1}sec^{-1}, a concentration C_b = 200 ng/mL, a flow rate v = 5 μm/sec, a saturation height H_{sat} = 3 nm, and a diffusion coefficient D = 40 μm^2/sec, which is typical for IgG molecules [39]. The cross sections of the protein spot for the experimental and simulation results are shown in Fig. 5(b), which shows similar profiles. The

#132716 - $15.00 USD Received 2 Aug 2010; revised 16 Sep 2010; accepted 17 Sep 2010; published 20 Sep 2010

simulated results match well with the experimental results at each time frame, validating the numerical simulation program.

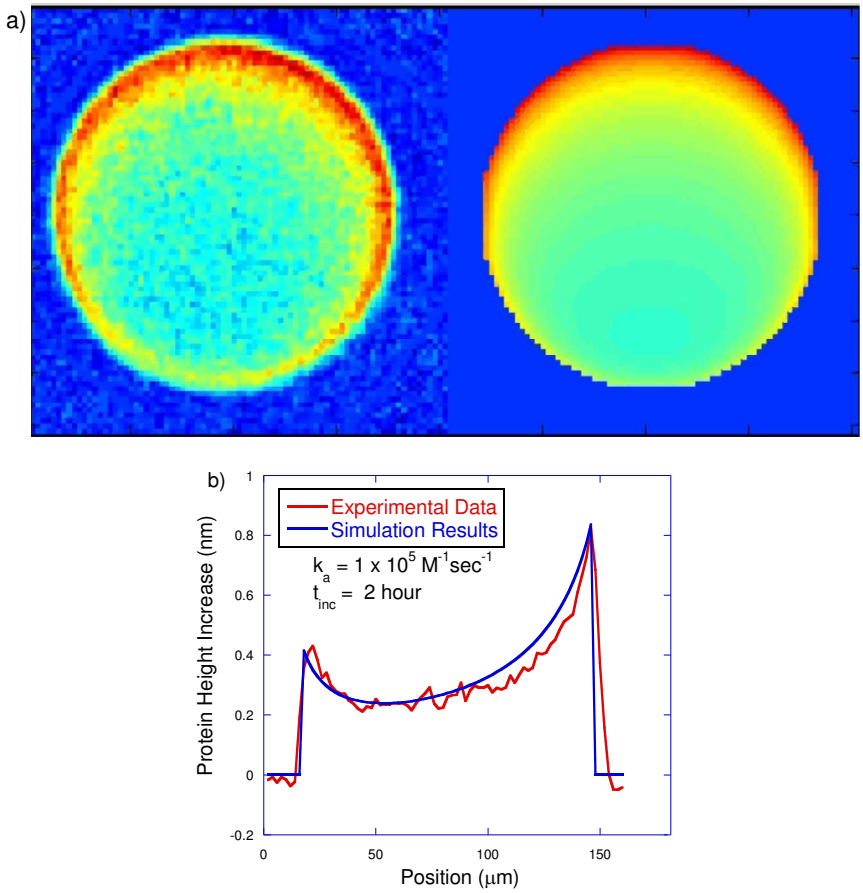

Fig. 5. Comparison of experimental and numerical simulation results. (a) (Media 2) A movie comparing experimental data and simulation of rabbit IgG binding against protein A/G. (b) Cross sections of the experimental and numerical data after 2 hour incubation.

4.3 Binding profile shapes

To study the effects of bulk concentration and flow velocity on the shape of the binding profile, Eq. (4) and Eq. (8) are combined. The concentration at the sensor surface is described by

$$\frac{\partial C}{\partial t} = -\vec{v}\cdot\nabla C + D\nabla^2 C - R\left(k_a C(H_{\max} - H) - k_d H\right) \qquad (11)$$

At low concentrations, the height profile of the protein binding is determined by the concentration gradient over the spot surface, which is dependent on both the mass transport of analyte and on the reaction kinetics. In Eq. (11), mass transport depends on the flow velocity and the diffusion coefficient, while the reaction kinetics depends on the association and dissociation rates, as well as the saturation height of the reaction. All of these factors affect the concentration gradient across the spot and the resulting spot binding profile. In particular, at low concentrations the condition $C_{bulk} << RH_{max}$ holds, which leads to low binding height H, and the concentration C in the fluid changes much faster than the surface protein height H. Therefore, H can be treated as slowly varying and small compared to $H_{\max}$. In this case, a

#132716 - $15.00 USD Received 2 Aug 2010; revised 16 Sep 2010; accepted 17 Sep 2010; published 20 Sep 2010

stable concentration gradient is established across the protein spot. In the limit of $H << H_{max}$, when the protein spot is far from saturation, the shape of the relative concentration gradient is independent of the analyte concentration.

Figure 6(a) shows the simulated surface height increase across the protein spot along the direction of the flow after a 1000 second incubation, normalized by the height of the leading edge to compensate for concentration differences. The parameters used for the simulations are k_a = 1x10^5 M^{-1}sec^{-1}, D = 40 μm^2/sec, saturation height H_{max} = 3 nm, and flow velocity v = 50 μm/sec. The bulk concentrations were varied from 10 ng/mL to 10 μg/mL. Except for the highest concentration, in which the reaction was driven close to saturation over the incubation time, at lower concentrations the height changes have very similar shape after normalization, which shows that the underlying mass transport and binding kinetics are independent of concentration in the low-concentration limit.

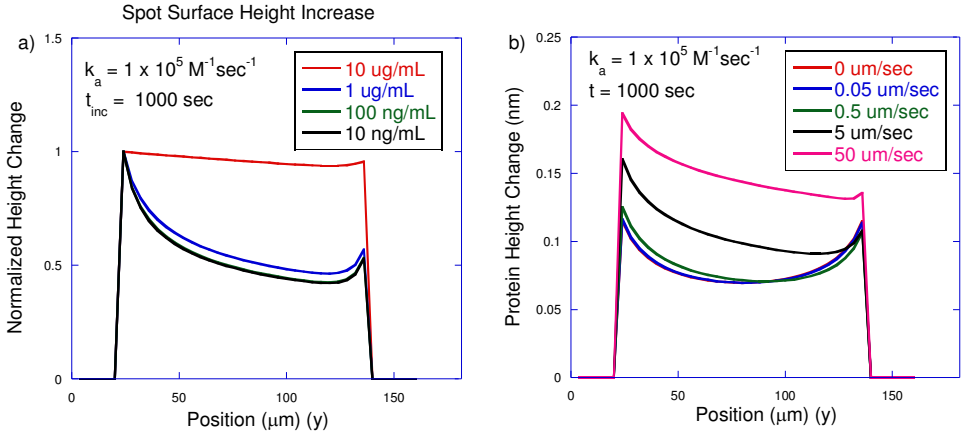

Fig. 6. (a) The normalized protein binding height at different concentrations across a spot. Except at the highest concentration, the others have similar normalized concentration profile. (b) Effect of active flow on the inhomogeneous binding profile of a protein spot after 1000 seconds incubation.

Figure 6(b) shows the effect of flow rate on the binding profile. The concentration is set at 1 μg/mL, the k_a is set at 1x10^5 M^{-1}sec^{-1}, the diffusion coefficient is set at 40 μm^2/sec, the saturation height set at 3 nm, and the flow rate changes from 0 to 50 μm/sec. The incubation time is set at 1000 seconds. The flow increases binding at the leading edge of the spot, and the width of the leading edge increases as the velocity of the flow increases. Higher association rates and saturation heights lead to a stronger binding term in Eq. (11), which increases the ratio between the center and the edge, and decreases the width of the edges. Higher diffusion and flow increase the mass transport term in Eq. (11), which decreases the ratio between the center and the edge, and increases the width of the edges.

4.4 Effect of mass transport on the time response

The inhomogeneous binding caused by mass-transport-limited reactions reduces the amount of captured analyte onto the antibody spots, thus decreasing the sensitivity of the assay. Figure 7(a) shows the average protein height change as a function of time under different flow rates. The concentration is set at 5 μg/mL, k_a is set at 1x10^5 M^{-1}sec^{-1}, the diffusion coefficient is set at 40 μm^2/sec, the saturation height is 1 nm, and the flow rate changes from 0 to 500 μm/sec. At high flow rate, the binding is close to ideal association, while for low flow rates insufficient mass transport leads to slower reaction and smaller binding signal. Figure 7(a) also shows the signal from the leading edge of the protein spots, in which depletion of analyte from the sample solution still results in deviation from ideal association, but the distortion is smaller compared to the average signal. These curves are fitted with an ideal response curve, and the resulting effective k_a values for both the average response and the leading edge

#132716 - $15.00 USD Received 2 Aug 2010; revised 16 Sep 2010; accepted 17 Sep 2010; published 20 Sep 2010

response are plotted in Fig. 7(b). The effective k_a values asymptotically approach the ideal value at $1x10^5$ $M^{-1}sec^{-1}$ with increasing flow velocity, while for low flow rates the binding process is dominated by diffusion mass transport, which leads to a much slower reaction rate. The effective k_a approaches the ideal k_a when the flow velocity exceeds a threshold value related to k_a and to the spot size. This critical velocity is discussed in the next section.

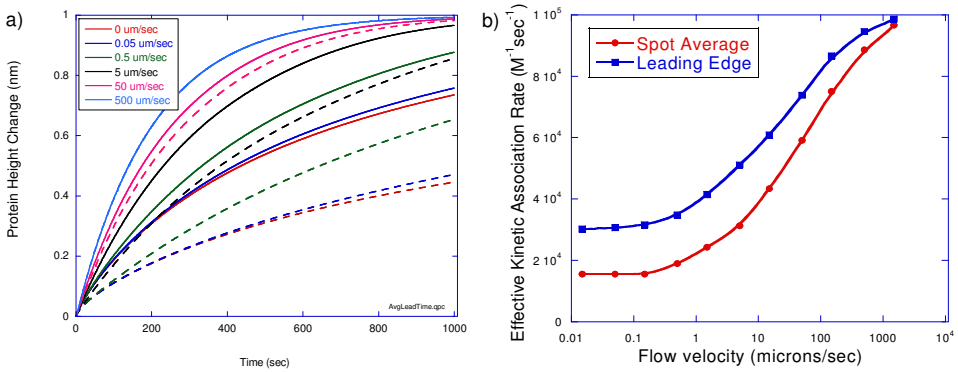

Fig. 7. Binding kinetics at different flow rates for 5 μg/mL. (a) The average response over a protein spot as a function of time (dashed curves) and at the leading edge of a protein spot as a function of time (solid curves). (b) Effective k_a for the average responses and the leading edge responses. The leading edge shows less deviation from ideal association, but is still strongly skewed from the ideal value at low flow rates.

5. Array performance guidelines

5.1 Optimal spot size

The depletion of analyte from solution adjacent to a protein spot results in concentration gradients over the same protein spot, which leads to inhomogeneous binding and reduced assay response. The length scale of the concentration gradient is determined by the reaction kinetics and mass transport conditions, and is independent of the size of the protein spots. Therefore, if we use protein spots with size comparable to, or smaller than, the length scale of the concentration gradient, then the entire spot would be exposed to nearly the bulk concentration of analyte, and mass transport limitations can be reduced. We first consider the case for pure diffusion mass transport (no flow). Equation (11), for $H << H_{max}$ and v = 0, becomes

$$\frac{\partial C}{\partial t} = D\nabla^2 C - Rk_a CH_{\max} \tag{12}$$

To simplify the problem for this set of conditions, only the one-dimensional case is considered. After a stable concentration gradient is established, then

$$D\frac{d^2C}{dx^2} - Rk_a CH_{\max} = 0 \tag{13}$$

and a characteristic length scale w_D can be defined for the concentration gradient. Equation (13) becomes

$$D\frac{C}{w_D^2} - Rk_a CH_{\max} = 0 \tag{14}$$

Because the diffusion-enhanced edge is caused by the concentration gradient, the width of the edge is the same as the decay length of the concentration gradient. Therefore the width of the diffusion edge is

#132716 - $15.00 USD Received 2 Aug 2010; revised 16 Sep 2010; accepted 17 Sep 2010; published 20 Sep 2010

$$w_D = \sqrt{\frac{D}{Rk_a H_{\max}}} \tag{15}$$

If the size of the protein spot is comparable to (or smaller than) w_D then the analyte concentration over the spot would not change significantly. Conversely, from this relation, if the association rate and saturation height are known, the diffusion coefficient of the analyte can be calculated from the width of the diffusion edge. By using the definition of R in Eq. (9), for an immunoassay with D = 40 μm^2/sec, ρ = 1.3 g/cm^3, k_a = 1x10^5 M^{-1}sec^{-1} and $H_{\max}$ = 3 nm, the calculated width of the diffusion edge is about 10 μm. This matches well with the experimental data at low flow rates in Fig. 5, in which the pixel resolution is 2.2 μm and the diffusion edge at the left and right of the spot parallel to the flow direction is about 4 pixels wide.

When active flow is added, and still considering only the one-dimensional case, Eq. (11) becomes

$$-v\frac{dC}{dx} + D\frac{d^2C}{dx^2} - Rk_a C H_{\max} = 0 \tag{16}$$

A characteristic length scale also can be associated with the flow term in Eq. (15), which then becomes

$$v\frac{C}{w_F} + D\frac{C}{w_D^2} - Rk_a C H_{\max} = 0 \tag{17}$$

If the contribution of the flow is larger than diffusion, the characteristic length scale of the concentration gradient w_F is given by

$$w_F \approx v / Rk_a H_{\max} \tag{18}$$

If the size of the protein spot is comparable to (or smaller than) the width of the concentration gradient, then the mass transport limitations can also be minimized. By using the definition of R in Eq. (9), with a k_a of 1x10^5 M^{-1}sec^{-1}, a diffusion coefficient of 40 μm^2/sec and a saturation height of 3 nm, for a 5 μm/sec flow rate the width of the leading edge is about 12 μm, and at 50 μm/sec flow rate the width of the leading edge is about 120 μm, which is the same as the size of the protein microspot This agrees with the experimental data in Fig. 1, in which the 5 μm/sec flow rate produces a pronounced binding edge, while the 50 μm/sec flow rate leads to uniform binding across the spot.

Equation (18) can be used to estimate the critical flow velocity needed to prevent significant mass transport effects to obtain close-to-ideal association. This critical flow velocity is

$$v_{crit} \approx w_F Rk_a H_{\max} \tag{19}$$

As an example, for w_F = 100 μm diameter protein spot, this critical flow rate is about 40 μm/sec, which agrees with the simulation results in Fig. 7 which shows a characteristic approach to saturation for flow velocities greater than 40 μm/sec.

This discussion provides an estimate of the length scale of the mass transport effect. The one-dimensional approximation is valid if an electrokinetically driven flow is used for the incubations, for which the flow velocity is a constant across the volume. In an experiment with pressure-driven flow, the parabolic velocity profile of the flow affects the size of the flow-enhanced edge. Figure 8 shows the simulated average spot height after a 1000 second incubation as a function of protein spot diameter, for (a) electrokinetically driven flow and (b) pressure driven flow. The kinetic association rate used for the simulations is 1x10^5 M^{-1}sec^{-1}, and the diffusion coefficient is 40 μm^2/sec. For the electrokinetically-driven flow, when the spot size is smaller than the length scale of the concentration gradient, no significant mass-transport limitation occurs. For the pressure driven flow, because the flow velocity close to

#132716 - $15.00 USD Received 2 Aug 2010; revised 16 Sep 2010; accepted 17 Sep 2010; published 20 Sep 2010

the surface is always slower, it is more susceptible to mass transport limitations. In either case, smaller protein spots lead to less distortion caused by mass-transport effects.

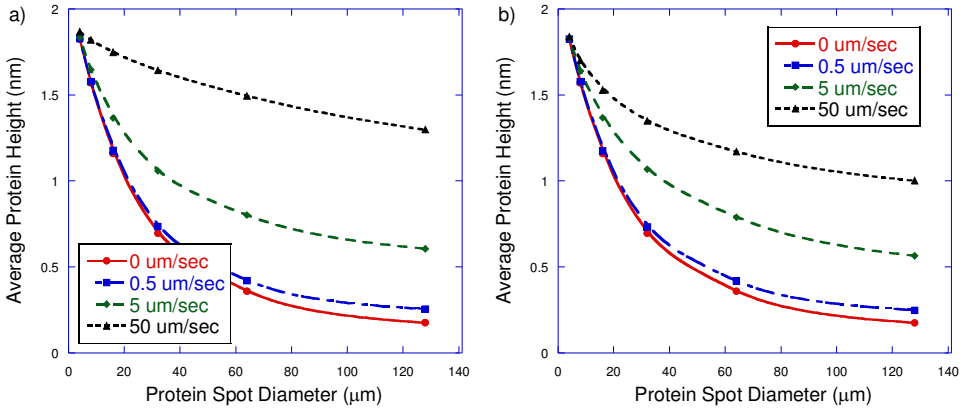

Fig. 8. Average protein height of protein spots with different sizes after 1000 second incubation at different flow rates for (a) electrokinetically driven flow and (b) pressure driven flow.

5.2 Utilizing mass-transport-limited reactions

One of the challenges for applying antibody microarrays to a complex biological sample such as serum or cell lysate is the distinction between specific reactions of low-concentration high-affinity target analytes and the non-specific binding of high-concentration low-affinity background proteins that are present in the biological sample. In the ideal association reaction given by Eq. (4), similar assay behaviors occur if the product k_aC = constant. On the other hand, as we have shown in Fig. 4, different association rates k_a lead to different height responses across a protein spot and to different degrees of distortion from ideal association in the time response. Therefore, these deviations provide experimental information that can be used to separate low-concentration-high-affinity from high-concentration-low-affinity reactions. For instance, Fig. 9(a) shows the simulated spot height of different reactions that hold the product of k_a and C constant at $k_a[C]$ = 0.005 sec^{-1} for an incubation time of 200 seconds. From the spatial shape of the response height, high association rate reactions result in much larger inhomogeneity. Figure 9(b) shows the average spot height of the binding, with higher k_a (consequently smaller [C]) leading to more distortion from ideal kinetics and slower rates. While it is possible to use kinetic time responses to distinguish specific and non-specific reactions, we suggest that it is more sensitive to measure the spatial binding inhomogeneity across the protein spot. In the Experimental Results section, Fig. 4 showed an experimental demonstration that distinguished specific from non-specific reactions. The higher-affinity reaction of avidin-biotin produced much larger inhomogeneity than low-affinity non-specific binding of BSA against protein A/G. By operating in the mass-transport-limited regime and measuring the binding profile, one can obtain more detailed understanding of the reaction kinetics.

#132716 - $15.00 USD Received 2 Aug 2010; revised 16 Sep 2010; accepted 17 Sep 2010; published 20 Sep 2010

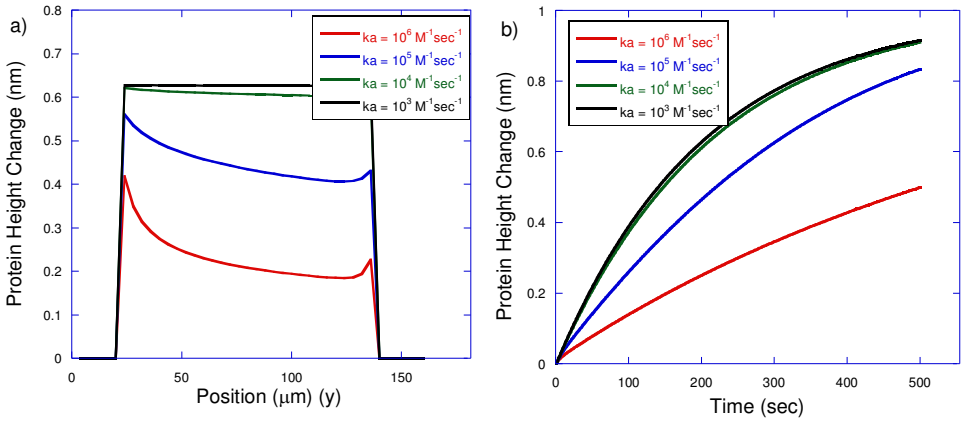

Fig. 9. (a) Binding profile within a protein spot and (b) binding kinetics at different kinetic association rates for $k_a[C]$ = 0.005 sec^{-1}. High association rate leads to larger inhomogeneity which can be easily distinguished from low association rate non-specific binding.

6. Conclusions

Mass-transport limitation is one of the key bottlenecks to the sensitivity of solid-support antibody microarrays. The common assay format of high-density antibody microspots is prone to local analyte depletion adjacent to the protein spots when the mass transport of analyte is too slow. The ambient-analyte assay condition dictates that the overall concentration of capture agent (when averaged over the volume within which analyte is transported to the surface) should be much smaller than the equilibrium concentration of analyte. Therefore, to limit assay deviations caused by mass transport rates, the local immobilized concentration must be small to prevent significant local analyte depletion. This requires either enhancing mass transport through faster flow velocity, or reducing the size of the microspot, both of which place constraints on the design of experiments.

As an alternative, in this paper we have shown that high-resolution molecular interferometric imaging (MI2) can measure spatially inhomogeneous binding profiles under mass-transport-limited conditions. The high spatial resolution of MI2 enables us to examine the effect of mass transport on an assay in greater detail than has been previously reported. By combining the experimental results of MI2 with a finite-element simulation program, we extracted accurate kinetic properties of the reaction, such as the diffusion coefficient of the analyte, as well as distinguishing among reactions with different association rates. We provided guidelines in the form of simple equations (rules of thumb) for designing optimal parameters of an assay system, such as spot size and flow rate, to limit the mass transport effects.

Acknowledgement

This work was sponsored by a research grant through Purdue Research Foundation from Quadraspec Inc. and the Indiana Economic Development Corporation. Funding was also from National Institutes of Health (NIH) NCI Grant No. R21CA125336.

#132716 - $15.00 USD Received 2 Aug 2010; revised 16 Sep 2010; accepted 17 Sep 2010; published 20 Sep 2010